

Ab-initio study of ultrafast charge dynamics in graphene

Q. Z. Li¹, P. Elliott¹, J. K. Dewhurst², S. Sharma¹ and S. Shallcross¹

1 Max-Born-Institute for Non-linear Optics and Short Pulse Spectroscopy,

Max-Born Strasse 2A, 12489 Berlin, Germany and

2 Max-Planck-Institut für Mikrostrukturphysik Weinberg 2, D-06120 Halle, Germany.

Monolayer graphene provides an ideal material to explore one of the fundamental light-field driven interference effects: Landau-Zener-Stückelberg interference. However, direct observation of the resulting interference patterns in momentum space has not proven possible, with Landau-Zener-Stückelberg interference observed only indirectly through optically induced residual currents. Here we show that the transient electron momentum density (EMD), an object that can easily be obtained in experiment, provides an excellent description of momentum resolved charge excitation. We employ state-of-the-art time-dependent density function theory calculations, demonstrating by direct comparison of EMD with conduction band occupancy, obtained from projecting the time propagated wavefunction onto the ground state, that the two quantities are in excellent agreement. For even the most intense laser pulses we find that the electron dynamics to be almost completely dominated by the π -band, with transitions to other bands strongly suppressed. Simple model based tight-binding approaches can thus be expected to provide an excellent description for the laser induced electron dynamics in graphene.

Intense laser light offers the possibility to control electrons in matter on femtosecond time scales. Triumphs of this burgeoning field include tuning the optically induced current in graphene via the carrier envelope phase of light¹⁻³, attosecond control over magnetic order in thin films of magnetic overlayers^{4,5}, and controlled valley excitation in the semi-conducting few layer dichalcogenides by circularly polarized light^{6,7} to name only a few examples. The two band Dirac cone found in graphene provides an ideal materials platform for studying one of the canonical light-field driven interference effects: Landau-Zener-Stückelberg (LZS) interference^{8,9}, which before its observation in graphene³ had only been observed in designed two state quantum systems¹⁰⁻¹⁴. This effect occurs when an oscillating electromagnetic field drives intraband oscillation through the Bloch acceleration theorem $\mathbf{k} \rightarrow \mathbf{k} + \mathbf{A}(t)/c$ and in the region of an avoided crossing interband transitions occur even when the band gap exceeds the dominant pulse frequency, so-called Landau-Zener transitions. Upon repeated passing of the avoided crossing multiple pathways exist to the conduction band with consequent constructive and destructive interference of electron states. This offers rich possibilities for controlling electron dynamics by intense laser light, demonstrated by the recent observation of control over optical currents underpinned by LZS interference³, a result anticipated theoretically in Ref. 15.

The ubiquity of the avoided crossing band structure in 2d materials, found not only in the Dirac cone of graphene but also in the the semi-conducting monolayer dichalcogenides¹⁶, phosphorene^{17,18}, silicene¹⁹, and stanene²⁰, points towards the importance of LSZ interferometry in controlling electron dynamics in 2d materials. However, while interference physics can be easily probed theoretically through the conduction band population^{18,21,22}, the experimental situation is more difficult, with to date only indirect observations of LSZ physics in materials reported. In this paper we show

that the transient electron momentum density (EMD) difference, defined as

$$\Delta\rho(\mathbf{p}, t_f) = \rho(\mathbf{p}, t_f) - \rho(\mathbf{p}, t = 0) \quad (1)$$

with \mathbf{p} momentum and $\rho(\mathbf{p}, t)$ the electron momentum density²³ before ($t = 0$) and after (t_f) the pump laser pulse, offers a tool for directly probing LZS interference effects. The EMD may be measured experimentally via tomographic reconstruction using Compton profiles²⁴⁻²⁸ and, in particular, for layered materials^{29,30}. Combining these techniques with ultrafast X-ray sources will allow the transient EMD to be experimentally measured. This suggests a way in which the LZS physics may be directly observed in 2d materials, opening the way to correlate indirect LZS physics such as induced currents with the fundamental momentum space interference patterns.

For graphene, we demonstrate that the EMD facilitates both the real time observation of the formation of LZS interference patterns, as well as the elucidation of subtle features in the relation between pump pulse and interference in momentum space.

In contrast to previous works that have employed simple single particle tight-binding Hamiltonians to study the LZS effect^{3,18,21,22,31-34}, we will here deploy the time dependent version of density functional theory (TD-DFT). To establish the accuracy of the EMD as a record of LZS interference we compare it with the excited electron distribution, N_{ex} , defined within TD-DFT as³⁵:

$$N_{\text{ex}}(\mathbf{k}, t) = \sum_i^{\text{occ}} \sum_j^{\text{unocc}} |\langle \psi_{i\mathbf{k}}(t) | \psi_{j\mathbf{k}}(t = 0) \rangle|^2 \quad (2)$$

where $\psi_{j\mathbf{k}}(t)$ is the time-dependent Kohn-Sham orbital at time t , and $\psi_{i\mathbf{k}}(t = 0)$ is the ground state orbital. In all cases we find that the pattern of excitation in momentum space generated by transient EMD and N_{ex} is nearly identical in the first BZ.

Finally, we consider the role of the non- π -band states in the electron dynamics in graphene. Remarkably, despite electron excitation through the whole energy range of the π -band (up to 10 eV above the Fermi energy, an energy range encompassing the σ^* bands as well as several high l character bands), it turns out that there occur almost no transitions to states outside the π -band manifold. We attribute this to the near vanishing of the corresponding dipole matrix elements. Our calculations thus suggest that even for very significant laser excitation tight-binding based models will provide a good description of the electron dynamics.

According to Runge-Gross theorem³⁶, which extends the Hohenberg-Kohn theorem into the time domain, with common initial states there will be a one to one correspondence between the time-dependent external potentials and densities^{37,38}. Based on this theorem, a system of non-interacting particles can be chosen such that the density of this non-interacting system is equal to that of the interacting system for all times, with the wave function of this non-interacting system represented by a Slater determinant of single-particle orbitals. These time-dependent Kohn-Sham (KS) orbitals are governed by the Schrödinger equation (for the spin degenerate case):

$$i\partial_t\psi_j(\mathbf{r},t) = \left[\frac{1}{2} \left(-i\nabla + \frac{1}{c} \mathbf{A}_{\text{ext}}(t) \right)^2 + v_s(\mathbf{r},t) \right] \psi_j(\mathbf{r},t). \quad (3)$$

In the above equation $\mathbf{A}_{\text{ext}}(t)$ is the vector potential representing the applied laser field, the effective potential $v_s(\mathbf{r},t)$ is given by $v_s(\mathbf{r},t) = v_{\text{ext}}(\mathbf{r},t) + v_{\text{H}}(\mathbf{r},t) + v_{\text{xc}}(\mathbf{r},t)$, where $v_{\text{ext}}(\mathbf{r},t)$ is the external potential, $v_{\text{H}}(\mathbf{r},t)$ the Hartree potential, and $v_{\text{xc}}(\mathbf{r},t)$ is the exchange-correlation (xc) potential. For the latter we have used the adiabatic local density approximation. From the Fourier transform of the Kohn-Sham states, $\psi_{i\mathbf{k}}(\mathbf{r})$, the electron momentum density can be constructed as $\rho(\mathbf{p}) = \sum_{i\mathbf{k}} |\psi_{i\mathbf{k}}(\mathbf{p})|^2$. This EMD constructed from KS states has been found to provide excellent agreement with that obtained from Compton scattering²³.

All calculations employ the state-of-the-art all-electron full potential linearized augmented plane wave (LAPW) method³⁹, as implemented in the ELK code⁴⁰. We have used a 30×30 \mathbf{k} -point set; for further details of the implementation of TD-DFT within the LAPW basis we refer the reader to Refs. 41 and 42.

LZS interference probed by 2D tr-EMD: the patterns of excited charge in momentum space that most directly characterise Landau-Zener-Stückelberg interference are generally presented by plotting the conduction band occupation over the first Brillouin zone. However this information, while easy to obtain theoretically, is difficult to obtain experimentally. We thus look at an alternative quantity, the change in electron momentum density due to the laser pulse.

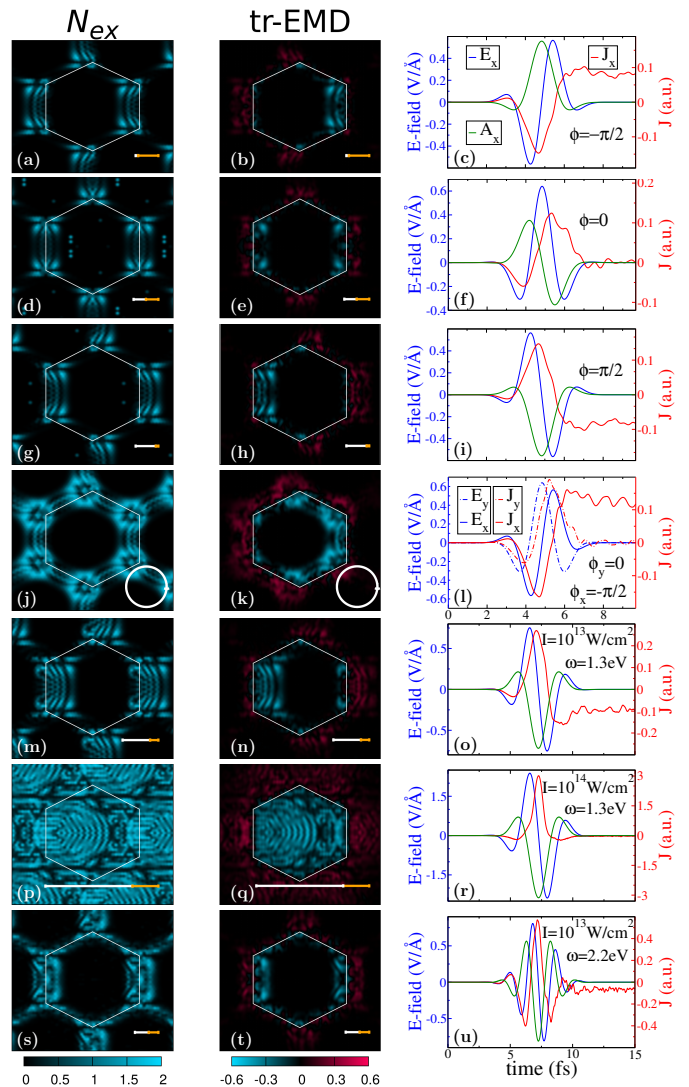


Figure 1: Conduction band occupation as a function of \mathbf{k} -vector as determined directly by projection of the time-dependent state onto the ground-state Kohn-Sham states (first column, see Eq. (2)), and, second column, the transient electron momentum density (tr-EMD) difference, see Eq. (1). Evidently, both quantities in a consistent way capture the momentum space intensity fringes generated by Landau-Zener-Stückelberg interference. The third column displays the electric field (\mathbf{E} -field) of the pump laser pulse (blue lines), the \mathbf{A} -field scaled such that it can be plotted on the same axis (green lines), and the induced current density (red lines). Pulses in (a)-(l) have a full width half maximum (FWHM) of 1.935 fs, a central frequency of 1.4 eV, and peak intensity of 5.43×10^{12} W/cm², and carrier envelope phase as indicated in the panels. The remaining three rows have FWHM 2.758 fs, CEP of $\pi/2$, and central frequencies and intensities as indicated in the panels. In the first and second columns, the white hexagons represent the boundary of the 1st BZ while the lines in the right bottom corner represent the effective \mathbf{k} -space trajectory given by the Bloch acceleration theorem.

In Fig. 1 are displayed the N_{ex} , EMD, and induced

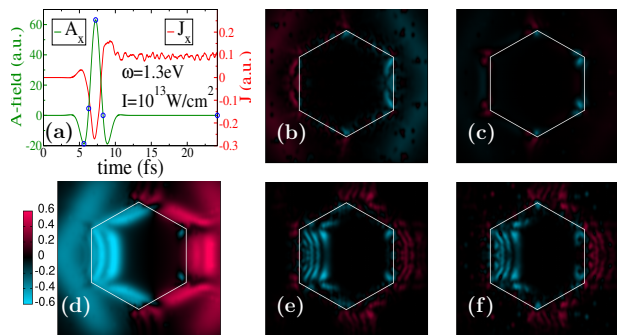


Figure 2: Landau-Zener-Stückelberg interference in the first Brillouin zone (BZ) reflected by 2D transient electron momentum density (tr-EMD) at various time steps during and after the pulse. A pulse of central frequency 1.3 eV, intensity 1.0×10^{13} W/cm², full width half maximum 2.758 fs, and carrier envelope phase $\pi/2$ is employed, with the \mathbf{A} -field exhibited and laser induced current exhibited in panel (a). The points on the \mathbf{A} -field curve indicate the times at which the tr-EMD is evaluated, shown in panels (b-f). In these panels the full evolution of the Landau-Zener-Stückelberg (LZS) interference can be seen, including both early time $k_x < 0$ (left hand side of the vertical BZ boundary line) conduction band excitation, intense excitation at the pulse peak, panel (d), before the development of the LZS interference fringes on the falling shoulder of the pulse, panel (e), and the full time $k_x > 0$ LZS interference.

currents for a diverse set of laser pulses exhibiting variation of several pulse parameters: carrier envelope phase (the angular difference between the \mathbf{E} -field and pulse envelope maxima), polarization, intensity, frequency, and full width half maximum (FWHM). The magnitude of the electric field is of the order of 5 V/nm, placing these pulses in the strong non-perturbative regime for graphene. As can be seen, in all cases N_{ex} and EMD convey consistent information concerning the excited charge, establishing the latter as a reliable probe of momentum space excitation.

Before exploring the LZS interference physics of graphene revealed in Fig. 1 we first provide a theoretical basis to this observed coincidence in the pattern of momentum space excitation between N_{ex} and EMD. The Kohn-Sham electron momentum density is defined as

$$\rho(\mathbf{p}, t) = \sum_{j\mathbf{k}} f_{j\mathbf{k}} |\psi_{j\mathbf{k}}(\mathbf{p}, t)|^2 \quad (4)$$

where

$$\psi_{j\mathbf{k}}(\mathbf{p}, t) = \int d\mathbf{r} e^{i\mathbf{p}\cdot\mathbf{r}} \psi_{j\mathbf{k}}(\mathbf{r}, t) \quad (5)$$

is the Fourier transform of the KS wavefunction $\psi_{j\mathbf{k}}$ and $f_{j\mathbf{k}}$ the occupation. Upon expansion of the Bloch functions in plane waves of the reciprocal lattice vectors, \mathbf{G} ,

$$\psi_{j\mathbf{k}}(\mathbf{r}, t) = \sum_{\mathbf{G}} c_{j\mathbf{G}}^{\mathbf{k}}(t) e^{i(\mathbf{k}+\mathbf{G})\cdot\mathbf{r}} \quad (6)$$

and insertion into Eqs. (4) and (5), we find that the EMD

can be expressed as

$$\rho(\mathbf{p}, t) = \sum_{j\mathbf{k}} f_{j\mathbf{k}} \sum_{\mathbf{G}} |c_{j\mathbf{G}}^{\mathbf{k}}(t)|^2 \delta(\mathbf{p} - \mathbf{k} - \mathbf{G}). \quad (7)$$

The EMD will therefore only change with respect to the ground-state EMD (see Eq. (1)) at points $\mathbf{p} = \mathbf{k} + \mathbf{G}$ where the coefficients $c_{j\mathbf{G}}^{\mathbf{k}}(t)$ change. In particular, in almost all systems, this will include the $\mathbf{G} = 0$ point, i.e. the \mathbf{k} point itself within the first Brillouin zone. As the coefficient, $c_{j\mathbf{G}=0}^{\mathbf{k}}(t_f)$, will change (w.r.t the GS value) at points in \mathbf{k} -space where $N_{\text{ex}}(\mathbf{k}, t_f)$ is non-zero, $\Delta\rho(\mathbf{k}, t_f)$ must also then be non-zero. Hence, any interference pattern seen in $N_{\text{ex}}(\mathbf{k}, t_f)$ will also be seen in $\Delta\rho(\mathbf{k}, t_f)$. For 2 electron systems, it is known that the EMD produced from the KS wavefunction can differ significantly from the exact EMD^{43,44}, however in periodic systems, it was shown that the KS-EMD gives excellent agreement with Compton Scattering profiles²³.

For a carrier envelope phase (CEP) of $\phi = \pm\pi/2$ the maximum \mathbf{E} -field intensity, and hence the interband transition at the avoided crossing, occurs at turning point of the path in momentum space executed due to the \mathbf{A} -field. As a result, the LZ transitions generate excited conduction band charge at either the positive ($\phi = +\pi/2$) or negative ($\phi = -\pi/2$) k_x sides of the Dirac point. This can be seen in rows (a-c) and (h-j) of Fig. 1. Note that positive and negative k_x , measured from the Dirac point, corresponds to the left and right hand sides of the vertical BZ boundary as seen in Fig. 1. In contrast, for $\phi = 0$ the maximum \mathbf{E} -field intensity occurs at $\mathbf{A} = \mathbf{0}$ resulting in a symmetric excitation about the Dirac point, see row (c-e). In the past such asymmetric LZS interference has been indirectly accessed by means the net current that results from the asymmetric momentum space occupation for non-zero CEP, and to date this represents the only observation in experiment of LZS in a material³. This coherent current (current per unit cell) induced by the laser pulse is displayed in the third column of Figs. 1 and 2, and corresponds well with that seen in experiment. The experimentally accessible EMD, however, provides a wealth of additional information, as we now describe.

By comparing rows (g-i) and (m-o) we observe almost identical residual coherent current, and yet a very different momentum space LZS excitation as revealed by the EMD. In particular, in row (m-o) we observe a subdominant $k_x < 0$ charge excitation absent in row (g-i) and reflecting multiple passes of the avoided crossing due to the side peaks of the former pulse, see panel (i). The presence of the main and side peaks in the pulse structure allows for multiple pass \mathbf{k} -space trajectories which, due to the pulse envelope, consist of a series of passes of the avoided crossing from trajectories of different length in momentum space. This yields both asymmetric occupation and more complex interference patterns. Further enhancement of these side peaks, see row (s-u) of Fig. 1 for which the CEP is again $\phi = +\pi/2$, results in well developed interference fringes both for positive and negative k_x , quite different to the right hand side only mo-

mentum space occupation seen for the lower frequency $\phi = +\pi/2$ pulse shown in panels (g-i). The EMD thus represents a much more sensitive probe of the LZS effect, able to unveil subtleties of the interference physics lost in the residual current.

A striking example of this richness of information provided by EMD versus the residual current can be found in rows (p-r). Here it can be seen that widespread excitation occurs throughout the BZ driven by an intense pulse the \mathbf{A} -field of which drives trajectories right across the BZ (indicated by the lines in the N_{ex} /EMD panels). A very complex and asymmetric LZS interference pattern results from this intense excitation, however the widespread occupation of momentum space drives an overall cancellation of current carrying states and a vanishingly small residual current.

Experimentally, the short time coherent current ultimately generates heating and a diffusive residual current. This can therefore not provide a real time probe of the development of LZS physics. Transient EMD, on the other hand, potentially provides a real time probe of the ultrashort time evolution of LZS interference patterns in momentum space. In Fig. 2 we show the transient EMD evaluated before, during, and after a pump pulse inducing both a coherent current and LZS interference. One can observe an early time excitation due to pulse side peaks, panels (b) and (c), followed by a dramatic excitation in momentum space at the maximum of the main peak, panel (d). Only after this peak has passed do the final interference fringes develop, panels (e) and (f).

Dominance of the π -manifold in electron dynamics: the results for the momentum resolved conduction band occupation shown in the previous sections, correspond very closely to results obtained on the basis of model π -band only tight-binding Hamiltonians. This raises the question of whether this is due simply to the relatively low energies of the excited charge (in Fig 1 and Fig. 2 the excited charge resides predominantly at the K point and the K-M-K line) or whether, for a more general reason, the π -band will always dominate ultrafast laser induced electron dynamics in graphene. To explore this in Fig. 3 we display the partial density of states calculated before and after the laser pulse. As can be seen, see Fig. 3a, for the pulse of intensity 10^{12} W/cm², the partial DOS after the pulse shows conduction band occupation only up to 2.5 eV. At these energies, see Fig. 3c, only the π -band is available for excited charge. Remarkably, when we consider a very strong pulse of intensity 10^{14} W/cm² the excited electrons are again only of p_z character, Fig. 3b, despite the fact that the laser pulse is sufficiently strong to excite charge from the minima of the π -manifold up to the maxima of the π^* -manifold. As may be noted from the band structure, Fig. 3c, within this energy range exist many other bands that would, in principle, be expected to be involved in the electron dynamics at such high energies. Examination of the relevant dipole matrix elements reveals that transitions from π to σ^* and π^* to σ are negligible for laser pulses with in-plane polariza-

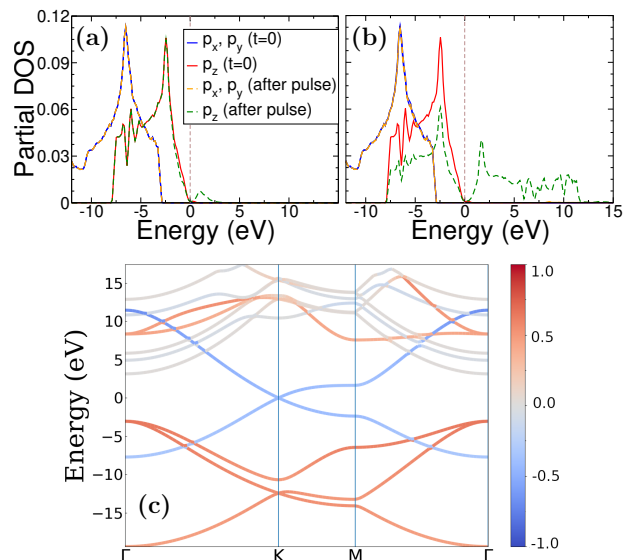


Figure 3: Time dependent partial density of states (PDOS) projected onto the $l = 1$ spherical harmonics. Here the PDOS (in states/atom/eV) is shown both at $t = 0$ before the pulse, and at the end of the simulation after the pulse has been applied. The pump pulse for panels (a) and (b) is polarized in the x -direction, with intensities 10^{12} W/cm² and 10^{14} W/cm² respectively. As can be seen, even for almost complete excitation of the π -band in which charge is excited from the π -band minima up to the π^* -band maxima, there is no excitation into states of p_x or p_y character. (c) Band structure of graphene showing the π and σ band character. Negative and positive numbers indicate dominance by π - and σ -character respectively.

tion. Thus even in the highly non-perturbative regime transitions from the ground state to the σ^* manifold will be strongly suppressed. It might be argued that the partial DOS, a projection within (touching) muffin tins, does not account for excitation to delocalized bands of high l character. Comparison of the interstitial density of states before and after the pulse shows that there is indeed an increase in interstitial charge at around 9 eV, possibly indicating transitions from the π^* manifold to delocalized bands (note the intersections between π^* and high l character bands on the M- Γ line), however this is a rather small effect. It would thus appear that the model π -band only tight-binding Hamiltonians provide an excellent description of the electron dynamics even for very intense laser pulses.

To summarize we have investigated *ab-initio* the laser induced electron dynamics in monolayer graphene. This system provides a canonical example of a material for which Landau-Zener-Stückelberg interferometry can be explored, and we have shown that direct visualisation of the interference fringes in momentum space is possible via the transient electron momentum density (EMD), establishing transient EMD as an excellent experimental tool for exploring LZS interference in 2d materials. Examination of the excited state partial density of states reveals that the π -band manifold decisively dominates ultrafast laser induced dynamics in graphene, justify-

ing the deployment of the popular Hückel tight-binding model. Whether this remains true for the complex few layer graphene systems, for which such an approach is the only one that can reasonably be envisioned, remains an open question.

I. ACKNOWLEDGEMENTS

QZL would like to thank DFG for funding through TRR227 (project A04). SS would like to thank DFG for

funding through SH498/4-1 and PE acknowledges funding from DFG Eigene Stelle project 2059421. The authors acknowledge the North-German Supercomputing Alliance (HLRN) for providing HPC resources that have contributed to the research results reported in this paper.

-
- ¹ Agustin Schiffrin, Tim Paasch-Colberg, Nicholas Karpowicz, Vadym Apalkov, Daniel Gerster, Sascha Mühlbrandt, Michael Korbman, Joachim Reichert, Martin Schultze, Simon Holzner, Johannes V. Barth, Reinhard Kienberger, Ralph Ernstorfer, Vladislav S. Yakovlev, Mark I. Stockman, and Ferenc Krausz. Optical-field-induced current in dielectrics. *Nature*, 493:70–74, 1 2013.
- ² Christian Heide, Takuya Higuchi, Heiko B. Weber, and Peter Hommelhoff. Coherent electron trajectory control in graphene. *Physical Review Letters*, 121:207401, 2018.
- ³ Takuya Higuchi, Christian Heide, Konrad Ullmann, Heiko B. Weber, and Peter Hommelhoff. Light-field-driven currents in graphene. *Nature*, 550:224–228, 2017.
- ⁴ John Kay Dewhurst, Peter Elliott, Sam Shallcross, Eberhard K. U. Gross, and Sangeeta Sharma. Laser-Induced Intersite Spin Transfer. *Nano Letters*, 18(3):1842–1848, March 2018.
- ⁵ Florian Siegrist, Julia A. Gessner, Marcus Ossiander, Christian Denker, Yi Ping Chang, Malte C. Schröder, Alexander Guggenmos, Yang Cui, Jakob Walowski, Ulrike Martens, J. K. Dewhurst, Ulf Kleineberg, Markus Münzenberg, Sangeeta Sharma, and Martin Schultze. Light-wave dynamic control of magnetism. *Nature*, 571:240–244, 7 2019.
- ⁶ Kin Fai Mak, Keliang He, Jie Shan, and Tony F. Heinz. Control of valley polarization in monolayer MoS₂ by optical helicity. *Nature Nanotechnology*, 7(8):494–498, August 2012. Number: 8 Publisher: Nature Publishing Group.
- ⁷ Hualing Zeng, Junfeng Dai, Wang Yao, Di Xiao, and Xiaodong Cui. Valley polarization in MoS₂ monolayers by optical pumping. *Nature Nanotechnology*, 7(8):490–493, August 2012. Number: 8 Publisher: Nature Publishing Group.
- ⁸ S.N. Shevchenko, S. Ashhab, and Franco Nori. Landau–zener–stückelberg interferometry. *Physics Reports*, 492:1–30, 7 2010.
- ⁹ Ya. I. Rodionov, K. I. Kugel, and Franco Nori. Floquet spectrum and driven conductance in dirac materials: Effects of landau-zener-stückelberg-majorana interferometry. *Phys. Rev. B*, 94:195108, Nov 2016.
- ¹⁰ Hugo Ribeiro, J. R. Petta, and Guido Burkard. Interplay of charge and spin coherence in landau-zener-stückelberg-majorana interferometry. *Phys. Rev. B*, 87:235318, Jun 2013.
- ¹¹ J. Stehlik, Y. Dovzhenko, J. R. Petta, J. R. Johansson, F. Nori, H. Lu, and A. C. Gossard. Landau-zener-stückelberg interferometry of a single electron charge qubit. *Phys. Rev. B*, 86:121303(R), Sep 2012.
- ¹² F. Forster, G. Petersen, S. Manus, P. Hänggi, D. Schuh, W. Wegscheider, S. Kohler, and S. Ludwig. Characterization of qubit dephasing by landau-zener-stückelberg-majorana interferometry. *Phys. Rev. Lett.*, 112:116803, Mar 2014.
- ¹³ E. Dupont-Ferrier, B. Roche, B. Voisin, X. Jehl, R. Wacquez, M. Vinet, M. Sanquer, and S. De Franceschi. Coherent coupling of two dopants in a silicon nanowire probed by landau-zener-stückelberg interferometry. *Phys. Rev. Lett.*, 110:136802, Mar 2013.
- ¹⁴ X. Mi, S. Kohler, and J. R. Petta. Landau-zener interferometry of valley-orbit states in si/sige double quantum dots. *Phys. Rev. B*, 98:161404(R), Oct 2018.
- ¹⁵ Kenichi L. Ishikawa. Electronic response of graphene to an ultrashort intense terahertz radiation pulse. *New Journal of Physics*, 15(5):055021, May 2013. Publisher: IOP Publishing.
- ¹⁶ A. C. Dias, Fanyao Qu, David L. Azevedo, and Jiyong Fu. Band structure of monolayer transition-metal dichalcogenides and topological properties of their nanoribbons: Next-nearest-neighbor hopping. *Phys. Rev. B*, 98:075202, Aug 2018.
- ¹⁷ Kiho Cho, Jiong Yang, and Yuerui Lu. Phosphorene: An emerging 2d material. *Journal of Materials Research*, 32(15):2839–2847, 2017.
- ¹⁸ Fatemeh Nematollahi, Vadym Apalkov, and Mark I. Stockman. Phosphorene in ultrafast laser field. *Phys. Rev. B*, 97:035407, Jan 2018.
- ¹⁹ Joelson C. Garcia, Denille B. de Lima, Lucy V. C. Assali, and João F. Justo. Group iv graphene- and graphane-like nanosheets. *The Journal of Physical Chemistry C*, 115(27):13242–13246, 2011.
- ²⁰ Yong Xu, Binghai Yan, Hai-Jun Zhang, Jing Wang, Gang Xu, Peizhe Tang, Wenhui Duan, and Shou-Cheng Zhang. Large-gap quantum spin hall insulators in tin films. *Phys. Rev. Lett.*, 111:136804, Sep 2013.
- ²¹ Hamed Koochaki Kellardeh, Vadym Apalkov, and Mark I. Stockman. Graphene in ultrafast and superstrong laser fields. *Phys. Rev. B*, 91:045439, Jan 2015.
- ²² Hamed Koochaki Kellardeh, Vadym Apalkov, and Mark I. Stockman. Attosecond strong-field interferometry in graphene: Chirality, singularity, and berry phase. *Phys. Rev. B*, 93:155434, Apr 2016.
- ²³ D Ernsting, D Billington, T D Haynes, T E Millichamp, J W Taylor, J A Duffy, S R Giblin, J K Dewhurst, and S B Dugdale. Calculating electron momentum densities

- and compton profiles using the linear tetrahedron method. *Journal of Physics: Condensed Matter*, 26(49):495501, nov 2014.
- ²⁴ Y. Sakurai, Y. Tanaka, A. Bansil, S. Kaprzyk, A. T. Stewart, Y. Nagashima, T. Hyodo, S. Nanao, H. Kawata, and N. Shiotani. High-resolution compton scattering study of li: Asphericity of the fermi surface and electron correlation effects. *Phys. Rev. Lett.*, 74:2252–2255, Mar 1995.
- ²⁵ L. Dobrzyński and A. Holas. Reconstruction of the electron momentum density distribution by the maximum entropy method. *Nuclear Instruments and Methods in Physics Research Section A: Accelerators, Spectrometers, Detectors and Associated Equipment*, 383(2):589 – 600, 1996.
- ²⁶ W. Schülke, G. Stutz, F. Wohlert, and A. Kaprolat. Electron momentum-space densities of li metal: A high-resolution compton-scattering study. *Phys. Rev. B*, 54:14381–14395, Nov 1996.
- ²⁷ G. Kontrym-Sznajd, M. Samsel-Czekala, S. Huotari, K. Hämäläinen, and S. Manninen. Fermi-surface mapping from compton profiles: Application to beryllium. *Phys. Rev. B*, 68:155106, Oct 2003.
- ²⁸ N. Hiraoka, T. Buslaps, V. Honkimäki, J. Ahmad, and H. Uwe. Fermi surface nesting in $Ba_{1-x}K_xBiO_3$ observed by compton scattering: Three-dimensional momentum density reconstruction study. *Phys. Rev. B*, 75:121101, Mar 2007.
- ²⁹ N. Hiraoka and T. Nomura. Electron momentum densities near dirac cones: Anisotropic umklapp scattering and momentum broadening. *Scientific Reports*, 7(1):565, 2017.
- ³⁰ F. F. Kurp, Th Tschentscher, H. Schulte-Schrepping, J. R. Schneider, and F. Bell. 3D-electron momentum density of graphite. *Europhysics Letters*, 35:61–66, 1996.
- ³¹ Hamed Koochaki Kelardeh, Vadym Apalkov, and Mark I. Stockman. Wannier-stark states of graphene in strong electric field. *Physical Review B - Condensed Matter and Materials Physics*, 90, 2014.
- ³² François Fillion-Gourdeau, Denis Gagnon, Catherine Lefebvre, and Steve MacLean. Time-domain quantum interference in graphene. *Physical Review B*, 94(12):125423, September 2016. Publisher: American Physical Society.
- ³³ C. Lefebvre, D. Gagnon, F. Fillion-Gourdeau, and S. MacLean. Carrier-envelope phase effects in graphene. *JOSA B*, 35(4):958–966, April 2018.
- ³⁴ Denis Gagnon, Joey Dumont, François Fillion-Gourdeau, and Steve MacLean. Pulse shaping in the terahertz frequency range for the control of photo-excited carriers in graphene. *Journal of the Optical Society of America B*, 35(12):3021, December 2018.
- ³⁵ P. Elliott, T. Müller, J. K. Dewhurst, S. Sharma, and E. K. U. Gross. Ultrafast laser induced local magnetization dynamics in Heusler compounds. *Scientific Reports*, 6:38911, December 2016.
- ³⁶ Erich Runge and E. K. U. Gross. Density-functional theory for time-dependent systems. *Phys. Rev. Lett.*, 52:997–1000, Mar 1984.
- ³⁷ C. A. Ullrich. *Time-Dependent Density-Functional Theory Concepts and Applications*. Oxford University Press, Oxford, New York, 2011.
- ³⁸ M.A.L. Marques, N.T. Maitra, F. Nogueira, E.K.U. Gross, and A. Rubio. *Fundamentals of Time-Dependent Functional Theory*. Springer-Verlag, Berlin, Heidelberg, 2012.
- ³⁹ D. J. Singh. *Planewaves Pseudopotentials and the LAPW Method*. Kluwer Academic Publishers, Boston, 1994.
- ⁴⁰ J. K. Dewhurst, S. Sharma, and et al., Jan. 14 **2018**.
- ⁴¹ K. Krieger, J. K. Dewhurst, P. Elliott, S. Sharma, and E. K. U. Gross. Laser-induced demagnetization at ultrashort time scales: Predictions of tddft. *Journal of Chemical Theory and Computation*, 11(10):4870–4874, 2015.
- ⁴² J.K. Dewhurst, K. Krieger, S. Sharma, and E.K.U. Gross. An efficient algorithm for time propagation as applied to linearized augmented plane wave method. *Computer Physics Communications*, 209:92 – 95, 2016.
- ⁴³ A.K. Rajam, Paul Hessler, Christian Gaun, and Neepa T. Maitra. Phase-space explorations in time-dependent density functional theory. *Journal of Molecular Structure: THEOCHEM*, 914(1):30 – 37, 2009. Time-dependent density-functional theory for molecules and molecular solids.
- ⁴⁴ Peter Elliott and Neepa T. Maitra. Electron correlation via frozen gaussian dynamics. *The Journal of Chemical Physics*, 135(10):104110, 2011.